IEEE J. Quantum Electronics 99, 2017, to appear – Personal Version, 31 December 2016

Synchronized Laser Chaos Communication: Statistical Investigation of an Experimental System

Anthony J. Lawrance, Theodore Papamarkou and Atsushi Uchida, *Member, IEEE*

***Abstract*—The paper is concerned with analyzing data from an experimental antipodal laser-based chaos shift-keying communication system. Binary messages are embedded in a chaotically behaving laser wave which is transmitted through a fiber-optic cable and are decoded at the receiver using a second laser synchronized with the emitter laser. Instrumentation in the experimental system makes it particularly interesting to be able to empirically analyze both optical noise and synchronization error as well as bit error rate. Both the noise and error are found to significantly depart in distribution from independent Gaussian. The conclusion from bit error rate results is that the antipodal laser chaos shift-keying system can offer a feasible approach to optical communication. The non-Gaussian optical noise and synchronous error results are a challenge to current theoretical modelling.**

***Index Terms*— Chaos, Semiconductor laser, Noise, Synchronization, Optical communication, Bit error rate**

I. Introduction

The area of synchronized laser-based communication developed rapidly after the demonstration of the communication use of chaos synchronization in electronic circuits [1,2]. The subsequent work over the next decade was surveyed in two special parts of IEEE journals, covering laser synchronization and cryptography aspects [3] and covering electronic circuit aspects [4]. Early works on numerical simulations [5-7] and experimental demonstration [8,9] of laser chaos communication were reported and a larger scale international demonstration [10,11] and high-speed transmission over Gb/s were studied [12,13]. Comprehensive book-length accounts of laser-based chaos communication have been published [14,15], which develop the area and discuss a wide range of systems and their implementations. From the electronic circuits perspective, there are several monographs covering a great variety of theoretical work in digital chaos communications [16,17]. Most give approximate theoretical developments and simulation analyses but do not cover experimental work.

A. J. Lawrance is with the Department of Statistics, University of Warwick, Coventry, CV47AL, U.K. (e-mail: A.J.Lawrance@warwick.ac.uk).

T. Papamarkou is with the School of Mathematics and Statistics, University of Glasgow, Glasgow G12QQ, Scotland. (e-mail: Theodore.Papamarkou @glasgow.ac.uk).

A. Uchida is with the Department of Information and Computer Sciences, Saitama University, 225 Shimo-Okubo, Sakura-ku, Saitama City, Saitama, 338-8570, Japan (e-mail: auchida@mail.saitama-u.ac.jp).

In this paper, we design a chaos-based communication experiment to investigate the effectiveness, in an optical experimental environment, of the antipodal chaos shift-keying system, first proposed using electronic circuits in [18,19]. The shift-keying idea has been implemented in a in a variety of communication settings, including laser-based secure communication [7] and laser on-off communications [20]. The non-coherent antipodal version of chaos shift-keying differs from chaos shift-keying as described in the classification (chaos masking, chaos modulation, and chaos shift-keying), introduced in [15]. In this class of chaos shift-keying, emitter and receiver lasers can switch parameter values between binary settings. The transmitted segment is then compared with each of the corresponding synchronized segments to determine which value has been sent. The antipodal chaos shift-keying system here involves an antipodal binary modulation of the emitter laser spreading segment and a synchronized segment, but is not chaos masking or chaos modulation according to the classification, neither of which involves spreading segments.

In the system of this study, transmission of a binary bit is by binary sign-modulation spread over of a segment of emitter laser output. The key components of the present non-coherent chaos shift-keying system are an emitter laser, a 60 km fiber-optic cable to a receiver and a receiver laser synchronized to the emitter laser. The focus of the paper is empirical, mainly concerned with revealing the statistical properties exhibited by the light intensity outputs of the lasers while they are experimentally transmitting binary bits, and using them to empirically assess the bit error performance of the chaos shift-keying system. The results also suggest appropriate theoretical assumptions which might be made in realistic base-band modelling of optical noise and synchronization error. Three outputs are measured in the experiment - the output of the emitter laser, a received modulated version of the emitter output incorporating hidden binary message bits after passing through the optical cable, and thirdly, a reference version of the emitter output at the receiver obtained by remote synchronization. The latter two outputs allow the binary message bits to be retrieved at the receiver by a correlation decoder. The emitter output is solely used to study optical noise and synchronization error in the experiment and not for decoding. The outputs were converted into voltages and then sampled at equi-spaced time intervals. This resulted in three time series waves of 10 Mega-point measurements, on an arbitrary scale.

These extensive data provide detailed information and the usual mathematically-based simulation of an assumed communication model can be replaced by empirical use of the experimental data. Bit error rate of the correlation decoder can be examined as a function of the spreading length of the sign-modulated segments of the emitter laser output. The statistical distributions and dependency of optical noise and synchronization are also revealed. Perhaps unexpectedly, they are both found to be non-Gaussian and dependent, with synchronization error the more strongly non-Gaussian. Moreover, their statistical dependency on the transmitter laser series is identified. Hence both types of wave are far from being independent Gaussian in distribution. The empirical results suggest, nevertheless, that the optical non-coherent chaos shift keying system can perform with suitably small bit error rate.

In earlier theoretically exact work [21], an antipodal chaos shift-keying system was studied involving transmission of emitter output instead of its synchronization; a single channel with independent Gaussian noise was assumed. These assumptions were broadened in [22] to give an exact BER result for dependent channel noise and dependent synchronization error with Gaussian assumptions and to give an approximate result based on second-order distributional properties. These give some insight into the empirical results of Section IV.B.

II. Experimental Details

A. *Experimental Setup*

Fig. 1 shows the experimental setup for chaos synchronization and communication. Two distributed-feedback (DFB) semiconductor lasers (optical wavelength 1547 nm) are used. One laser is used as an emitter and the other as a receiver. The injection current and temperature of each semiconductor laser are adjusted by a controller. The optical wavelength of the semiconductor lasers is precisely controlled by the temperature of the laser with a ratio of 0.097 nm/K. The resolution of the temperature control is 0.01 K. The injection currents of the lasers are set to 15.20 mA (the emitter) and 12.00 mA (the receiver), respectively, where the lasing thresholds of injection current I_{th} are 10.57 mA (the emitter) and 9.38 mA (the receiver). The relaxation oscillation frequencies of the lasers are 3.0 GHz (the emitter) and 2.0 GHz (the receiver), respectively. Each of the two lasers is prepared without standard optical isolators, to allow optical feedback and injection.

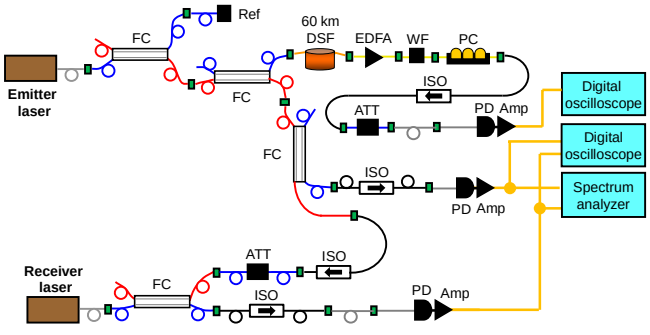

Fig. 1 Schematics of the laser-based communication experiment. Amp, electronic amplifier; ATT, optical attenuator; 60 km DSF, 60 km dispersion-shifted fiber; EDFA, erbium-doped fiber amplifier; FC, fiber coupler; ISO, optical isolator; PC, polarization controller; PD, photodetector; Ref, fiber reflector; WF, wavelength filter.

The emitter laser is connected to a fiber coupler and a variable fiber reflector which reflects a fraction of the light back into the laser, inducing high-frequency chaotic oscillations of the optical intensity. The amount of the optical feedback light is adjusted by the variable fiber reflector. The fiber length between the emitter laser and the variable fiber reflector is 4.55 m, corresponding to the feedback delay time (round-trip) of 43.8 ns. On the other hand, there is no optical feedback for the receiver laser. Polarization maintaining fibers are used for all the optical fiber components, except a long-distance optical fiber.

The output of the chaotic emitter laser is divided into two beams by a fiber coupler. One of the emitter beams is injected into the receiver laser to achieve synchronization. An optical fiber isolator is used to achieve one-way coupling from the emitter to the receiver lasers. The injection power is adjusted by using an optical attenuator. The wavelengths of the two lasers are precisely matched in order to achieve optical injection locking, which is a necessary condition for synchronization. The injection locking range is 0.073 nm (9.1 GHz) in this experiment. The optical wavelength of the receiver laser is slightly tuned within the injection locking range to obtain the maximum cross-correlation of temporal waveforms between the two lasers.

The optical outputs of the two lasers are converted into electronic voltage signals by using high-speed AC-coupled photodetectors (New Focus, 1554-B, 12 GHz bandwidth). The converted electronic signals are amplified by electronic amplifiers (New Focus, 1422-LF, 20 GHz bandwidth). The two electronic signals are sent to a high-speed digital oscilloscope (Tektronix, DPO71604B, 16 GHz bandwidth, 50 GigaSamples/s) and a radio frequency (RF) spectrum analyzer (Agilent, N9010A-526, 26.5 GHz bandwidth) to observe temporal waveforms and RF spectra, respectively, of the two laser outputs for synchronization.

The other emitter beam is transmitted through a 60-km-long dispersion-shifted fiber (DSF) for the detection of an optical noise signal via a communication channel. After the transmission, the light power is amplified by an erbium-doped fiber-optical amplifier (EDFA). The center wavelength is extracted at around 1.5 μm by using a wavelength filter. The polarization direction of each beam is adjusted by a polarization controller (PC). The beam is attenuated by an optical attenuator to adjust the detection power. The beam is injected to another photodetector and an electronic amplifier, and detected by another digital oscilloscope (Tektronix, DPO71254, 12.5 GHz bandwidth, 50 GS/s). Two oscilloscopes are used for this experiment, since the lag time between the transmitted signal and the emitter laser output is very large (~ 0.3 ms) due to the 60-km fiber transmission. A trigger function is used for the detection of high peak values of the chaotic waveforms to match the timing of the two signals detected by the two oscilloscopes.

B. Experimental Data Adjustment

Three 10 Mega-point long series of voltage intensity signals were obtained during experimental transmissions: $\{X_t\}$ the *emitter wave* from the emitter laser, $\{R_t\}$ the *received emitter wave* after transmission through the 60 km long-distance fiber-optic cable and $\{S_t\}$ the *synchronized emitter wave* at the receiver. The received emitter wave is modelled as

$$R_t = X_t + \varepsilon_t \tag{1}$$

where $\{\varepsilon_t\}$ is *optical noise*. The optical noise originates from 60-km fiber transmission and the following optical amplification through EDFA. In fact, $\{\varepsilon_t\}$ consists of the optical noise and electronic noise from the photodetector and oscilloscope. However, we consider that the optical noise is dominant in $\{\varepsilon_t\}$ since two temporal waveforms of the emitter and receiver lasers are very similar without long fiber transmission and optical amplification.

The synchronized emitter wave is modelled as

$$S_t = X_t + \eta_t \tag{2}$$

where $\{\eta_t\}$ is *synchronization error*. It follows from (1) and (2) that optical noise and synchronization error are

$$\varepsilon_t = R_t - X_t \tag{3}$$

and

$$\eta_t = S_t - X_t, \tag{4}$$

respectively. The calculated data of these latter two quantities allow the study of their statistical distributions and dependencies as would be needed in realistic base-band mathematical modelling.

In chaos shift-keying communication use, as to be described in Section II.C, segments of the emitter wave are modulated by antipodal binary messages before transmission and become *message segments*, based on R_t .

The recording of the experimental data required the use of two photo detectors with different sensitivities. There were instrumental processing effects, manifesting in artificially different amplitudes which needed correction. Statistical scaling was used and the received message and synchronized series are adjusted in amplitudes to that of the emitter series. The desired result is that an adjusted message signal R_t should be the addition of its emitter signal and an adjusted optical noise ε_t, that is

$$R_t' = X_t + \varepsilon_t' . \tag{5}$$

This can be achieved by regressing R_t on X_t to obtain the coefficients α_R, β_R and the adjusted variables

$$R_t' = (R_t - \alpha_R)/\beta_R, \quad \varepsilon_t' = \varepsilon_t/\beta_R . \tag{6}$$

These variables satisfy the additivity in Eq.(5). The adjusted optical noise is then

$$\varepsilon_t' = R_t' - X_t. \tag{7}$$

In a similar manner, for an adjusted synchronized emitter S_t' to have the same amplitude as the emitter X_t and a corresponding synchronization error η_t' , that is

$$S_t' = X_t + \eta_t' \tag{8}$$

the required adjusted variables are

$$S_t' = (S_t - \alpha_S)/\beta_S, \quad \eta_t' = \eta_t/\beta_S . \tag{9}$$

Then the adjusted synchronization error is

$$\eta_t' = S_t' - X_t. \tag{10}$$

The subsequent graphical analysis is entirely in terms of the variables $\{X_t, R_t', S_t'\}$ and the derived optical noise $\{\varepsilon_t'\}$ and laser synchronization error $\{\eta_t'\}$.

C. Antipodal Chaos Shift-Keying Communication Scheme

According to antipodal chaos shift-keying communication, transmitting a binary message $b = \pm 1$ involves multiplying the bit value into a *segment* of the emitter wave to create a *spreading segment* $b\{X_t\}$ which is then transmitted and received as a *message segment* $\{R_t\}$. The synchronized version of the emitter segment, $\{S_t\}$, usually called a *reference segment*, is also available at the receiver. There will be a chosen number N of successive intensity measurements in each of the three segments; N is known as the *spreading factor* and its size is an important factor which controls bit error. Hence, for communicating a bit b, the equations describing the message and reference segments are

$$\{R_t\} = b\{X_t\} + \{\varepsilon_t\}, \ \{S_t\} = \{X_t\} + \{\eta_t\} \tag{11}$$

corresponding to Eq. (5) and Eq.(8) and where {} denote segments in this equation.

The basic idea is to decode the binary bit by comparing the message segment voltages with the corresponding synchronized emitter segment voltages; generally similar segments imply $b = 1$ and sign-reversed segments imply $b = -1$. Security of laser-based systems is stenographic [15], with a transmitted binary bit being hidden by its multiplication into the emitter wave. A correlation decoder is used to decode the transmitted bit on the basis of the message and synchronized emitter segments; it is a statistical estimate which is the sign of the correlation between the voltages of the message and synchronized segments. In the absence of optical noise and synchronization error, the message and synchronized segments should be equal, or of opposite sign. Correct bit retrieval is inhibited by both noise $\{\varepsilon_t\}$ from the long-distance fiber-optic cable and error $\{\eta_t\}$ from the synchronization method. These effects will be statistically assessed in Sections III.D and III.B, and the main communication aspects will be covered in Section IV.

The transmission process is repeated consecutively for each bit of an entire message.

To allow the study of optical noise and synchronization error in the experiment, transmission is limited to +1 bits; by symmetry of the system this is not a restriction when investigating bit error.

IEEE J. Quantum Electronics 99, 2017, to appear – Personal Version, 31 December 2016

III. Statistical Displays of Experimental Results

A. Emitter and Synchronized laser Signals

The nature of the experimental outputs is best seen initially from stretches of their adjusted intensity values in time series plots. Fig. 2 gives a typical stretch of 250 values from the emitter laser output $\{X_t\}$ and the synchronized output $\{S'_t\}$, both starting at the time index position 5000001. The level of both series appear constant, a conclusion supported by other stretches which have been examined. Further, there does not appear to be changes in amplitude, or any obvious periodicity. Thus an initially tenable assumption without considering dependency, is that the series are statistically stationary. The close tracking of the two series is evidence of their synchronization, with the differences representing synchronization error $\{\eta'_t\}$.

The next aspect to be considered is the marginal distributions of the emitter and synchronized series, $\{X_t\}$ and $\{S'_t\}$, respectively; these are given by the histograms in Fig.3. The means are each very near zero, both being -0.000120, and the standard deviations are 0.086823, 0.0938630, respectively. The emitter series histogram in Fig. 3(a) indicates that the emitter laser does not generate Gaussian distributed values; they are negatively skewed, with coefficient -0.72. Negative skewness is also evident in the synchronized series histogram, Fig. 3(b), with coefficient -0.86. The differences between these histograms and the rather peculiar sharp maxima of the emitter laser and reference laser distributions, with excess3-kurtosis of (1.16,1.26), respectively, are likely to be instrumental effects. Note that the histograms are on the same scale in order to make meaningful visual comparisons. Autocorrelations of the emitter series are displayed in Fig. 3(c) and show linear dependency in the series with initially strong cyclic decreasing amplitudes over 15 lags, although this does not indicate strict cyclical behaviour in the series, rather it summarizes the oscillation behaviour. One lag corresponds to a 20 picoseconds sampling time of the oscilloscope. Autocorrelations of mean-adjusted squared series, not shown, indicate nonlinear dependency over the first 2 lags, with slight indications of cyclic behaviour thereafter. The synchronized series displays similar behaviour.

B. Synchronization Error

The synchronization errors $\{\eta'_t\}$ have been shown in Fig. 2 as the differences between the emitter and synchronized time series. Fig. 4(a) shows their distribution relative to a Gaussian distribution; they are strongly peaked over zero with a standard deviation of 0.035668, much smaller than 0.086823 of the emitter distribution. This points to acceptable levels of variation from a communications perspective. The non-Gaussian nature of the histogram is graphically evident and verified by its skewness and excess3-kurtosis (-0.56, 1.61), respectively, compared to zero Gaussian values. The general variability of the distribution can be appreciated from its range (-0.24,0.24) compared to the simulated range of a 10 Mega-point Gaussian random sample of the same mean and variance, (-0.19,0.19). The distribution has much more data in its longer tails than would be found with the corresponding fitted Gaussian distribution. Asymmetric departures from the 45-degree in the scatter Fig. 4(b) point to the non-Gaussian distribution of received values depending on the emitter values. The scatter

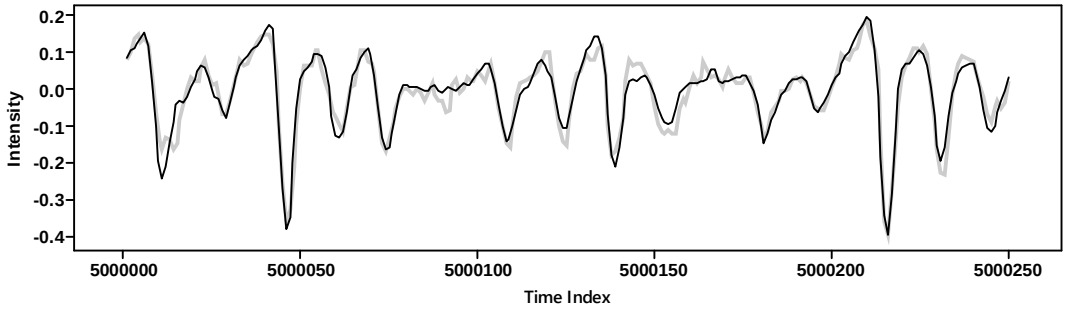

FIG. 2. A comparison of the emitter wave (thick grey line) and the synchronized wave at the receiver (thin black line) for the time index range 5,000,001:5,000,250; the differences depict synchronization error.

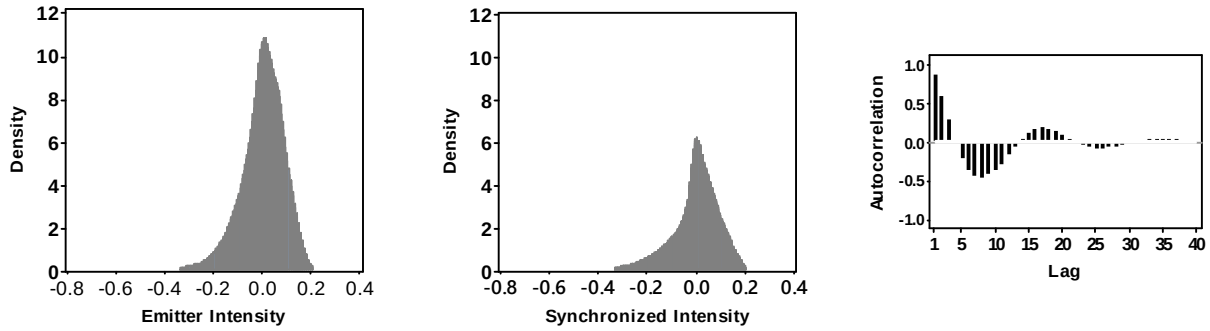

(a) (b) (c)

FIG. 3. (a) Distribution of the emitter intensity values. (b) Distribution of the synchronized emitter intensity values. (c) Autocorrelations of emitter intensity values.

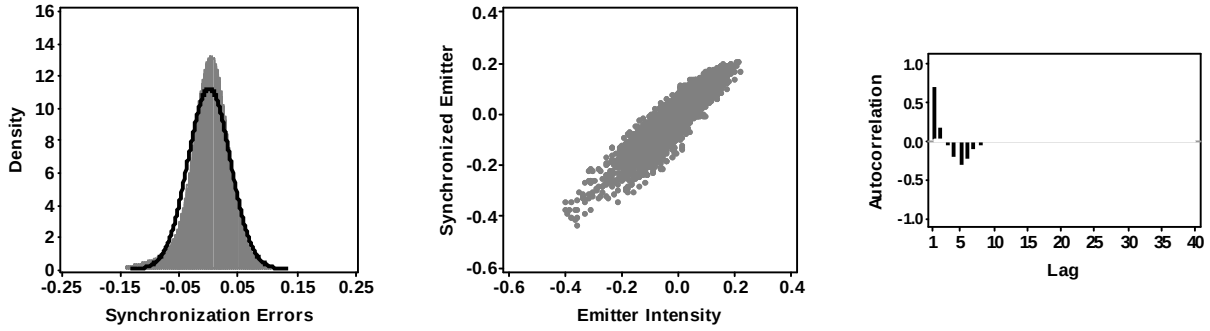

(a) (b) (c)

FIG. 4. (a) Histogram of the synchronization errors with its ill-fitting Gaussian distribution. (b) Scatter plot of 5,000 pairs (segment 5000001:5005000) of emitter values and synchronized and emitter values. (c) Autocorrelations of synchronization errors.

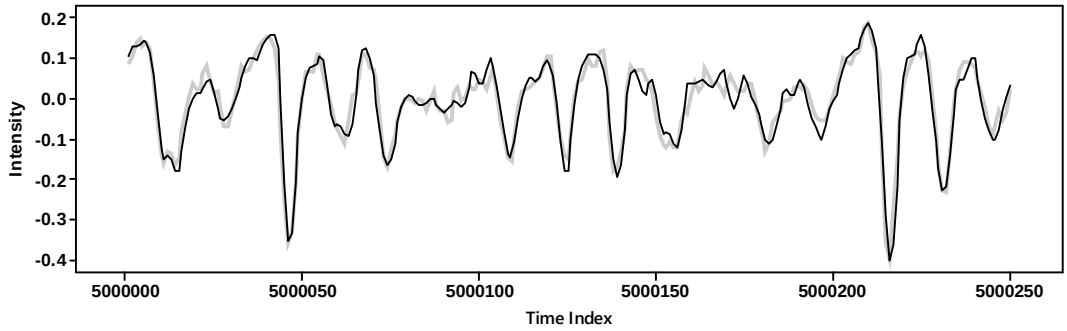

FIG. 5. Comparison of the emitter wave (thick grey line) and the received emitter wave (thin black line) for the time index range 5,000,001:5,000,250; the differences depict optical noise.

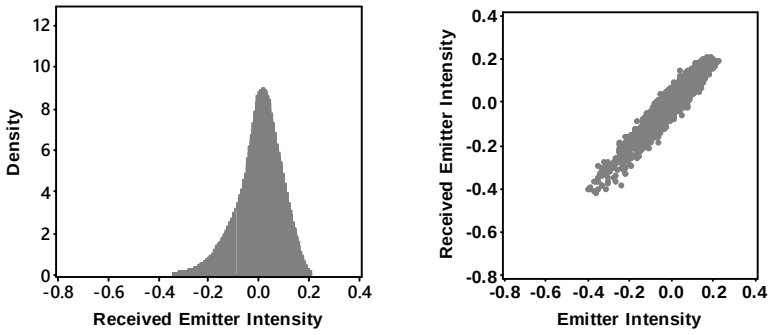

(a) (b)

FIG.6. (a) Distribution of the received emitter intensity values after transmission through the optical cable. (b) Scatter plot of 5,000 pairs (segment 5000001:500500) of emitter values and received emitter values.

over all 10 Mega-point synchronization pairs has a correlation of 0.925, strong but not perfect. Fig. 4(c) shows that synchronization errors are autocorrelated, and thus dependent. These properties are relevant when mathematical base-band modelling of the communication system.

C. Emitter Signals and Received Emitter Signals

The experimental system can be used to examine the statistics of binary bit transmissions through the long-distance fiber-optic cable. Binary bits of +1 are transmitted since they use the emitter transmissions without the need for modulation and there is binary symmetry; the received wave with binary +1 message wave is thus of the form given in Eq. (5). In Fig. 5 there is a typical stretch of 250 values of the emitter laser values $\{X_t\}$ and the received message values $\{R_t\}$, both starting at the time index position 5000001. Differences between the two series, $\{\varepsilon_t\}$, represent optical noise, but they are not extreme. The distribution of the received signals is shown by the histogram in Fig. 6(a), similar to the emitter distribution, Fig. 3(a), but modified by the effect of optical transmission noise. It has a mean near zero of –0.00012 and standard deviation of 0.092009, and skewness is -0.79. In Fig. 6(b) there is a scatter plot comparison of the received and emitter signals based on 5000 values. Asymmetric departures from the 45-degree line point to a non-Gaussian distribution of received values depending on the emitter values, while their slim scatter with a high correlation of 0.944 for all 10 Mega-point transmission

pairs is stronger than 0.925 for synchronization pairs.

D. Optical Noise

The distribution of optical noise for all 10 Mega-point values is depicted by the histogram in Fig. 7(a); the standard deviation is 0.030453, much smaller than the emitter standard deviation of 0.086823, and thus acceptable from a communications perspective. Also shown there is the somewhat inadequate fit of a Gaussian distribution. The skewness and excess3-kurtosis are (-0.11, 0.72), not strikingly high relative to their zero Gaussian values, and considerably less than those for synchronization errors. But it is again additionally informative to compare the range of the distribution (-0.31, 0.22) with that of a simulated 10 Mega-point Gaussian random sample of the same size, mean and variance, which was found to be (-0.15, 0.15). Thus, the distribution of optical noise has much more data in its longer and asymmetric tails than would be found in the symmetric tails of a best-fitting Gaussian distribution. Moreover, optical noise is autocorrelated and not independently distributed, a further departure from standard Gaussian assumptions. Fig. 7(b) gives its autocorrelations, showing strong values at the first lag and some slighter correlation at a few subsequent lags. These are perhaps effects which should be examined more widely. In summary, it can be said that the optical noise is not independent Gaussian noise and would need to be modelled with an appropriate distribution and dependency structure.

E. Dependency of Optical Noise and Synchronization Error on Emitter Signal

A possible reason for the autodependency of optical noise and that of synchronization error, as shown in Fig. 4(c) and Fig. 7(b), respectively, might be that they are both affected by their associated emitter signals. Investigating this involves obtaining their distributions conditional on the emitter signal values over a set of their intervals. A suitable graphic for this purpose using median, inter-quartiles and the outer adjacent points at 1.5 times the interquartile distance, is the boxplot, and is given in Fig. 8 for optical noise and for synchronization error; a boxplot of noise or error values is given for each interval of emitter values. Any pattern in these plots indicates dependency on emitter intensity.

For optical noise, the pattern in Fig. 8(a) points to the variability of the noise decreasing as the strength of the emitter signal increases, with the mean remaining fairly constant, except at the ends. It is plausible that the change in variability is a causative effect, although there does not appear to be any theoretical work which supports such a conjecture. The less consistent behavior of the outer few boxplots, particularly the change in medians, reflects the small amounts of data at the associated emitter values. For synchronization error, the strong pattern in Fig. 8(b) shows that the median error follows a mostly decreasing curve. Similar effects can be found with the

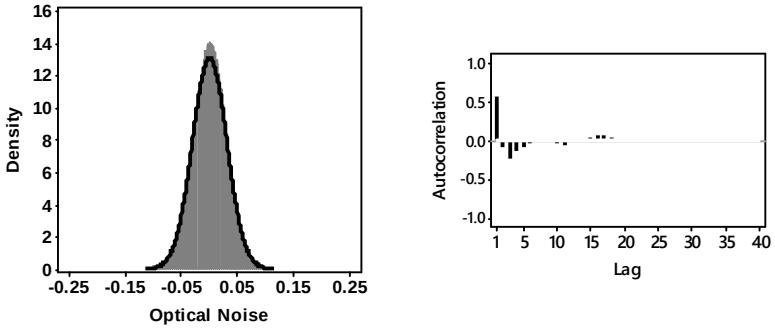

(a) (b)

FIG. 7. (a) Histogram of optical noise with its ill-fitting Gaussian distribution. (b) Autocorrelations of optical noise.

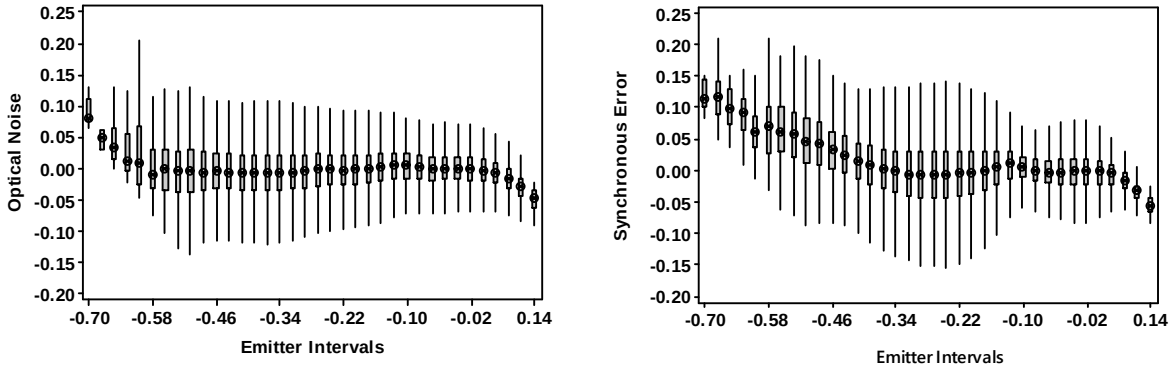

(a) (b)

FIG. 8. (a) Distribution boxplots of optical noise conditional on grouping of emitter laser intensity values. (b) Distribution boxplots of synchronization error conditional on grouping of emitter laser intensity values.

mean and standard deviations. These effects might also be thought of as causative, although again there does not appear to have been any theoretical analysis to support the conjecture.

The empirical results here suggest a possible development of the model Eqs. (1) and (2) as

$$R_t = bX_t + \varepsilon_t(X_t), \quad S_t = X_t + \eta_t(X_t) \qquad (12)$$

where the noise and errors are functions of the emitter signal as well as independent components. These functions would have to be obtained, either empirically or theoretically.

F. Statistics of Received and Synchronized Reference Signals

As mentioned in Section II.C, from a communications point of view, a transmitted binary bit is decoded at the receiver by comparing its received and synchronized segments using their correlation, with a low negative correlation for a -1 bit. Therefore a general comparison of all 10 Mega-point received emitter values and synchronized intensity values is of interest in relation to the transmission of a +1 bit. A superimposed time series plot of a section of length 250 from the two series is given in Fig. 9 and shows their strong similarity. The associated correlation over the entire series takes the high value 0.917.

From a communications perspective, a comparison of segment-sized lengths is most relevant, and scatter plot examples for $N = 10, 20, 50$ are given in Fig. 10. These correctly indicate decoding of +1 bits.

IV. Bit Error Rate Results from Experimental Transmissions

A. Bit Error Rate Results

The experimental system and its data outputs are a suitable basis for investigating the bit error rate of an antipodal chaos shift-keying system in its non-coherent version, similar to that treated by exact theory under Gaussian noise and error assumptions in [21]. A binary multiplicative operation ± 1 is applied to a spreading segment of successive emitter laser outputs after which it is transmitted through the long-distance fiber-optic cable to a receiver where it must be decoded. Correlation decoding is used in this analysis. By the setup of the experiment, only $+1$ segments are transmitted – so there is no actual sign changing to the emitter outputs. At the receiver there are available a series of 10 Mega-point emitter intensity values, deemed modulated by $+1$ bits and affected by optical noise, and a corresponding series of synchronized emitter intensity values, affected by synchronization error. For the purposes of bit error calculation, each of these 10 Mega-point long series are sub-divided in parallel into $10^7/N$ pairs of (R, S) spreading segments of extent N, $N = 2, 3, \ldots, 25$.

Bit error rate (BER) is empirically assessed by the proportion of segment pairs which are negatively correlated. The dependence of BER on the extent of spreading (N) is of obvious performance interest and will be displayed in this section and Section IV.B. More conventionally, BER is plotted against the

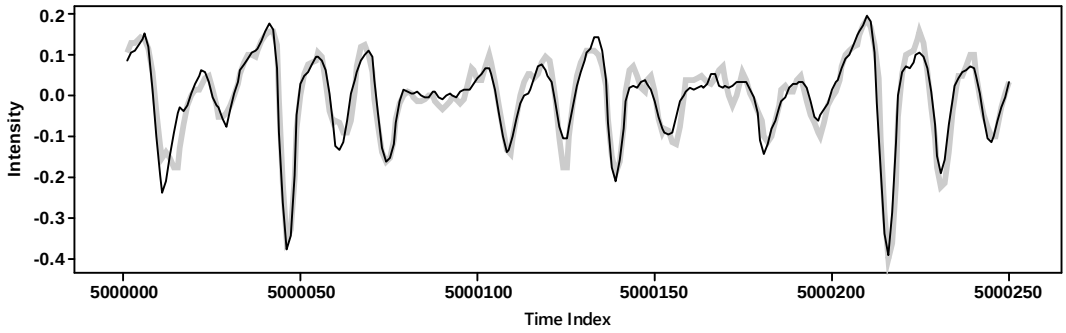

FIG. 9. Comparison of received emitter wave (thick grey line) and the corresponding synchronized wave (thin black line) for the time index range 5,000,001:5,000,250.

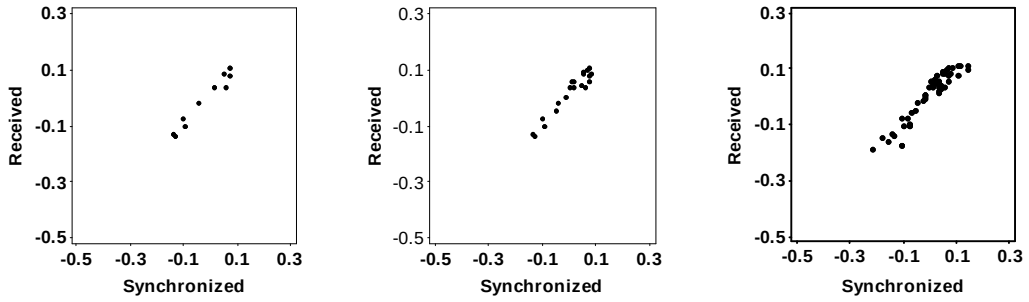

FIG. 10. Illustration of received and synchronized spreading segments for N=10, 20, 50 in (a), (b) and (c), respectively, as examples required in antipodal chaos shift-keying communication for decoding a +1 bit; the correlations of these spreading scatters are 0.994, 0.889, 0.949, respectively.

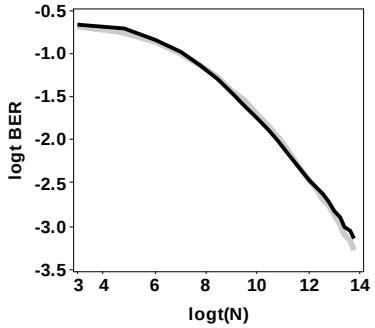

FIG. 11. BER curve of the coherent chaos shift-keying communication system in which there is no synchronization error at the receiver (thick black curve) and of the nearly coincident curve for the corresponding non-coherent system (thick grey curve). The calculations are based on the 10 Mega-point experimental data.

signal-to-noise ratio, but in the present system there are two signal ratios, one relative to optical noise and one relative to synchronization error, and both these are fixed by the experimental settings. Nevertheless, an empirical way of varying them will be suggested in Section IV.B.

Fig. 11 gives two curves which plot BER against a log transformation of N defined as $\log_{10}(N)$, a form which is suitable for comparisons, and gives curves of comparable shapes to signal-to-noise plots for coherent systems, as used for instance, in [16] and [21]. The thick grey curve is for the BER of the non-coherent system discussed previously and is seen to decrease satisfactorily as the spreading extent increases within the range of reliability when calculated from the available correlations. However, in the experimental situation, the non-coherent version may be compared with the coherent case as an empirical lower bound in which the synchronized segments are replaced by the corresponding experimentally known 'exact' segments; these are the 'synchronized' segments with no synchronization error. This is the coherent case of the system and is shown as the thick black decreasing curve in Fig. 11 which is initially slightly higher than the grey non-coherent curve, perhaps a slightly puzzling but empirical feature. However, by $N = 6, (\log_{10} N = 8)$ the thick grey curve has fallen slightly below the non-coherent black curve and continues to be just slightly lower until instability in the tails of the two curves becomes evident. Over the entire range the two curves are thus very close which implies that the practically relevant non-coherent system is performing near its empirical optimum, even for modest spreading. The synchronization achieved is thus strong enough for communication purposes.

B. Influence of Optical Noise and Synchronization Error on Bit Error Rate

It has been noted in Section IV.A that there are two signal ratios of importance, one relative to optical noise and one relative to synchronization error. These involve their standard deviations which cannot be easily changed experimentally since they are consequences of the length of the long-distance fiber-optic cable and the synchronization properties of the two lasers, respectively. To vary them experimentally would require considerable further resources, for instance, experiments with different lengths of optical cable. An alternative empirical statistical strategy is suggested here which involves creating artificial data sets made from the original experimental data but with increased or decreased variability of the optical noise and or synchronization error. This is equivalent to varying the pair of signal ratios. Working from the adjusted noise values $\{\varepsilon_t'\}$ with a scaling factor $1+\alpha$, and adjusted synchronization error values $\{\eta_t'\}$ with a scaling factor $1+\beta$, where $-1 \le \alpha, \beta < \infty$, the new adjusted received and synchronized emitter waves can be constructed as

$$R_t'' = X_t + (1+\alpha)\varepsilon_t', \;\; S_t'' = X_t + (1+\beta)\eta_t', t = 1,2,...,10^7. \quad (13)$$

Bit error calculations can now be carried out on the constructed waves for various choices of α and β. This approach is empirical but does have the statistical advantage of retaining the empirical distribution shapes and the dependency found in the experimental optical noise and synchronization error.

Initially, attention is restricted to changing optical noise and so $\beta = 0$ is assumed and the synchronization error is kept at its experimental level. Calculation of BER remains as in Section IV.A. In Fig. 12(a) the black BER curve is for the experimental non-coherent case ($\alpha = 0, \beta = 0$). The upper three well-separ ated grey curves give BER for increased optical noise with ($\alpha = 0.25, 0.50, 1.0; \beta = 0$). Nearly coincident with the non-coherent black curve are three grey curves with no or reduced optical noise and experimental synchronization error ($\alpha = -1.0, -0.9, -0.1; \beta = 0$). Clearly, increased optical noise has strong detrimental effects on BER but reducing optical noise in the presence of experimental synchronization error has much less effect. The large detrimental effects could be moderated by increased spreading length and cost. In Fig. 12(b) optical noise is kept at its experimental level while the synchronization error level is changed. The effect is similar to that in Fig. 12(a), a consequence of symmetric treatment in the correlation decoder of optical noise and synchronization error. The lowest curves in both panels of Fig. 12 indicate that modest joint reduction of both optical noise and synchronization error ($\alpha = -0.25, \beta = -0.25$) is effective in reducing BER whilst strong reduction in one of these is almost ineffective. However, increasing just one by the same proportion does increase BER. Differences in level between the two panels of Fig. 12 are due to the strength of optical noise being less than that of synchronous error.

Fig. 13 deals with two further situations when there is only one type of disturbing behaviour, either optical noise or synchronization error. In each of these circumstances, the decrease of variability causes a pronounced reduction in BER, in contrast to when both optical noise and synchronization error are present when the reduction is slight.

The effects noted in Fig. 12 and Fig. 13 may be partially explained further by the approximate theoretical BER result,

$$BER \simeq \Phi\left\{-\sqrt{N}\left[\frac{\sigma_\varepsilon^2}{\sigma_X^2}\left\{1+\sum_{k=1}^{N}\left(1-\frac{k}{N}\right)\rho_X(k)\rho_\varepsilon(k)\right\}\right.\right.$$
$$+\frac{\sigma_\eta^2}{\sigma_X^2}\left\{1+\sum_{k=1}^{N}\left(1-\frac{k}{N}\right)\rho_X(k)\rho_\eta(k)\right\}$$
$$+\frac{\sigma_\varepsilon^2\sigma_\eta^2}{\sigma_X^4}\left\{1+\sum_{k=1}^{N}\left(1-\frac{k}{N}\right)\rho_\varepsilon(k)\rho_\eta(k)\right\}$$
$$\left.\left.+\frac{\sigma_{X^2}^2}{\sigma_X^4}\left\{1+2\sum_{k=1}^{N-1}\left(1-\frac{k}{N}\right)\rho_{X^2}(k)\right\}\right]^{-1/2}\right\}, \qquad (14)$$

where ρ is used for autocorrelation of the suffixed variable and Φ is the distribution function of a standardized Gaussian variable. This is a rearrangement of the result derived in [22, Eq. 52], to show behaviour in terms of *N*. The formula does not accommodate the empirical dependencies modelled by Eq. (12) but never-the-less allows some comparisons with previously described empirical results. The decreasing of BER with *N* is evident. The roles of the optical noise and synchronization error can also be seen in the separate terms of Eq. (14), particularly their individual and multiplicative effects which are in agreement with Fig.12 and Fig.13. The multiplicative effects in the autocorrelations give further insight into the effect of autocorrelation in the optical noise and synchronization error, and the last term shows the effect of nonlinear dependency from the emitter. More detailed comparisons would involve calculating summations in Eq. (14) for the experimental data, but exact comparisons are limited by the approximate nature of Eq. (14), and its main purpose is to identify the key quantities influencing BER values.

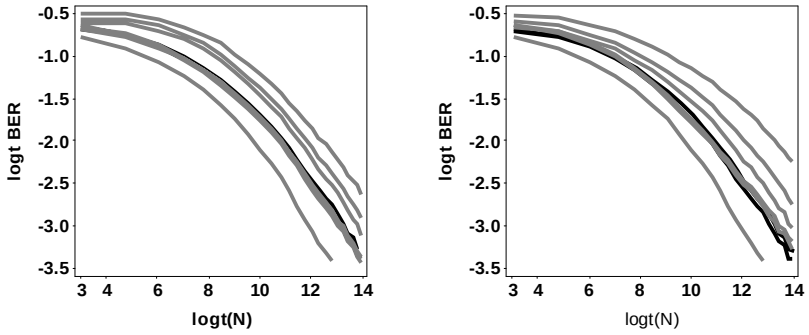

FIG. 12. BER curves for varying optical noise and synchronization error. (a) The upper three grey BER curves are for increased optical noise and experimental synchronization error $(\alpha = 0.25, 0.50, 1.0; \beta = 0)$ while the black curve is the experimental non-coherent original case, $(\alpha = 0; \beta = 0)$; the lower two almost coincident grey curves are also for only reduced optical noise $(\alpha = -0.1, -0.9; \beta = 0)$**.** The lowest curve is for simultaneous reduction of both optical noise and synchronization error $(\alpha = -0.25; \beta = -0.25)$. (b) The upper three grey *BER* curves are for increased synchronization error and experimental optical noise $(\alpha = 0; \beta = 0.25, 0.50, 1.0)$ while the black curve is for the experimental non-coherent original case, $(\alpha = 0; \beta = 0)$, and the lower two almost coincident grey curves are just for reduced synchronization error $(\alpha = 0; \beta = -0.1, -0.9)$**.** The lowest curve is for simultaneous reduction of both optical noise and synchronization error $(\alpha = -0.25; \beta = -0.25)$.

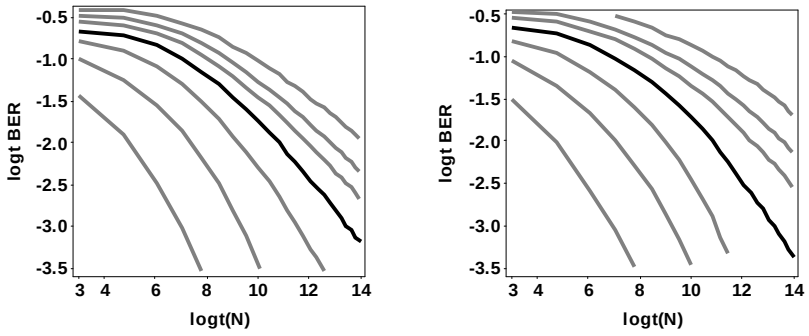

FIG. 13. (a) *BER* curve (black) for no optical noise and experimental synchronization error, $(\alpha = -1; \beta = 0)$, and six *BER* curves (grey) for no optical noise and changing levels of synchronization error. The upper three grey curves are for increased synchronization error $(\alpha = -1; \beta = 0.25,\ 0.50, 1.0)$ while the three lower ones are for reduced synchronization error $(\alpha = -1; \beta = -0.25, -0.5, -0.75)$**.** (b) *BER* curve for no synchronization error (black), the coherent case $(\alpha = 0; \beta = -1)$**,** and six *BER* curves (grey) for changing levels of optical noise. The upper three curves (grey) are for increased optical noise $(\alpha = 0.25, 0.50, 1.0; \beta = -1)$ while the three lower ones are for reduced optical noise $(\alpha = -0.25, -0.5, -0.75; \beta = -1)$**.**

The graphics in this section represent an attempt to gain maximum information from the experimental data set which is of communication interest. The basic statistical presumption has been that the distributional dependency behaviour in the experimental data is maintained after making changes to the variances of the optical noise and synchronization error. The empirical approach offers a number of further possibilities. A surface of bit error in respect of the standard deviations of optical noise and synchronization error could be obtained; this should better reveal their interaction. Comparison with Gaussian noise and errors could also be studied.

V. Conclusions

In summary, an experiment was conducted to investigate the feasibility of a non-coherent antipodal chaos shift-keying system of communication using optical channels and chaos synchronization. An empirical analysis of the experimental data confirmed the feasibility of such a system and its satisfactory performance in terms of bit error. Statistical properties of the system were found to be quite distinct from the Gaussian properties of conventional electronic circuit versions, a point of importance for future theoretical modelling. Detailed statistical analysis of the experimental data revealed that optical noise and synchronization errors were distributed with skewness and kurtosis, and more importantly were autocorrelated and nonlinearly dependent; both of them were found to be satisfactorily small, with optical noise being the lesser. Synchronization error was small enough for the system to perform very near its coherent BER lower bound. An empirical statistical methodology was presented for examining the effect of varying the strength of the optical noise and synchronization error without new experimentation. This pointed to several effects, such as the modest reduction of both of these being more effective in reducing BER than a strong reduction of either. The empirical methodology approach could be of wider laser communication interest when experimentation is restricted by resources or time.

Acknowledgment

The authors are appreciative of the early contributions from Dr Chibisi Chima-Okereke, formerly of Active Analytics, Bristol, U.K., in programming and scoping parts of the initial statistical analysis; they are also grateful to Hiroki Aida, Saitama University, for his experimental contribution. AU acknowledges support from Grants-in-Aid for Scientific Research from Japan Society for the Promotion of Science, and Management Expenses Grants from the Ministry of Education, Culture, Sports, Science and Technology in Japan. AJL acknowledges support from the UK Engineering and Physical Sciences Research Council via the Centre for Research in Statistical Methodology of the University of Warwick.

References

[1] L. M. Pecora and T. L. Carroll, "Synchronization in chaotic systems," *Physical Review Letters*, vol. 64, pp. 821-824, 1990.

[2] T. L. Carroll and L. M. Pecora, "A circuit for studying the synchronization of chaotic systems," *International Journal of Bifurcation and Chaos*, vol. 3, pp. 659-667, 1992.

[3] S. Donati and C. M. Mirasso, "Introduction to the feature section on optical chaos and applications to cryptography," *IEEE Journal of Quantum Electronics* vol. 38, pp. 1138-1140, 2002.

[4] M. Hasler, G. Mazzini, M. Ogorzalek, M. Rovatti, and G. Setti, "Scanning the special issue - special issue on applications of nonlinear dynamics to electronic and information engineering," *Proceedings of the IEEE*, vol. 90, pp. 631-640, 2002.

[5] P. Colet and R. Roy, "Digital communication with synchronized chaotic lasers," *Optical Letters*, vol. 19, pp. 2056-2058, 1994.

[6] C. R. Mirasso, P. Colet, and P. García-Fernández, "Synchronization of chaotic semiconductor lasers: application to encoded communications," *IEEE Photonics Technology Letters*, vol. 8, no. 2, pp. 299-301, 1996.

[7] V. Annovazzi-Lodi, S. Donati, and A. Scirè, "Synchronization of chaotic injected-laser systems and its application to optical cryptography," *IEEE Journal of Quantum Electronics*, vol. 32, no. 6, pp. 953-959, 1996.

[8] G. D. VanWiggeren and R. Roy, "Communication with chaotic lasers," *Science*, vol. 279, no.5354, pp. 1198-1200, 1998.

[9] J.-P. Goedgebuer, L. Larger, and H. Porte, "Optical cryptosystem based on synchronization of hyperchaos generated by a delayed feedback tunable laser diode," *Physical Review Letters*, vol. 80, no. 10, pp. 2249-2252, 1998.

[10] A. Argyris, D. Syvridis, L. Larger, V. Annovazzi-Lodi, P. Colet, I. Fisher, *et al.*, "Chaos-based communications at high bit rates using commercial fibre-optic links," *Nature*, vol. 438, pp. 343-346, 2005.

[11] A. Argyris, A. Bogris, M. Hamacher, and D. Syvridis, "Experimental evaluation of subcarrier modulation in chaotic optical communication systems " *Optics Letters*, vol. 35 pp. 199-201, 2010.

[12] A. Argyris, E. Grivas, M. Hamacher, A. Bogris, and D. Syvridis, "Chaos-on-chip secures data transmission in optical fibre links," *Optics Express*, vol. 18, pp. 5188-5198, 2010.

[13] R. Lavrov, M. Jacquot, and L. Larger, "Nonlocal nonlinear electro-optic phase dynamics demonstrating 10 Gb/s chaos communications," *IEEE Journal of Quantum Electronics*, vol. 46, no. 10, pp. 1430-1435, 2010.

[14] J. Ohtsubo, *Semiconductor Lasers: Stability, Instability and Chaos*, Third Edition, Springer-Verlag, Berlin Heidelberg 2013.

[15] A. Uchida, *Optical Communications with Lasers - Applications of Nonlinear Dynamics and Synchronization*. Weinheim: Wiley-VCH, 2012.

[16] F. C. M. Lau and C. K. Tse, *Chaos-based Digital Communications Systems*. Heidelberg: Springer Verlag, 2003.

[17] W. M. Tam, F. C. M. Lau, and C. K. Tse, *Digital Communications with Chaos*. Oxford: Elsevier, 2007.

[18] U. Parlitz and S. Ergezinger, "Robust communication based on chaotic spreading sequences," *Physics Letters A*, vol. 188, pp. 146-50, 1994.

[19] G. Kolumban, B. Vizvari, W. Schwarz, and A. Abel, "Differential chaos shift keying: a robust coding for chaotic communication," in *Nonlinear Dynamics of Eletronic Systems*, Seville, Spain, 1996, pp. 87-92.

[20] A. Uchida, S. Yoshimori, M. Shinozuka, T. Ogawa, and F. Kannari, "Chaotic on-off keying for secure communications," *Optics Letters*, vol. 26, pp. 866-868, 2001.

[21] A. J. Lawrance and G. Ohama, "Exact calculation of bit error rates in communication systems with chaotic modulation," *IEEE Transactions on Circuits and Systems I: Fundamental Theory and Applications*, vol. 50, pp. 1391-1400, 2003.

[22] A. J. Lawrance, "Communicating with chaos: a case of statistical engineering," *Statistical Science*, 31, 558-577, 2016.

Anthony J. Lawrance received the B.Sc., MSc. and Ph.D. degrees in Mathematics, Statistics and Mathematical Statistics, in 1963, 1964 and 1969 from University of Leicester, University of Wales and University of Leicester, U.K., respectively.

In 1965, he joined the Department of Mathematics at the University of Leicester as a Tutorial Assistant and Assistant Lecturer, while undertaking Ph.D. research. He was a Visiting Staff Member at the IBM Thomas J. Watson Research Center, New York, USA, 1970-71. In 1974 he joined the Department of Statistics at the University of Birmingham, U.K., where he was successively Lecturer, Senior Lecturer, Reader and Professor, moving to the University of Warwick, U.K. in 2004, currently

as Emeritus Professor. He has held several visiting university positions in Australia, Japan and Australia. Present research activity is in the statistical aspects of chaos communication, financial statistical modelling and applications of statistics in engineering areas.
Dr Lawrance is a Fellow and former Vice-President of the Royal Statistical Society, and former Honorary Secretary of its Research Section and Chairman of its West Midlands region.

Theodore Papamarkou received the B.Sc. degree in Mathematics from the University of Ioannina, Greece, in 2000, the M.Sc. and Ph.D. degrees in Statistics from the University of Warwick, U.K. in 2004 and 2010, respectively.

In 2010, he worked in the Department of Public Health and Primary Care, University of Cambridge, U.K., as a post-doctoral research associate in statistical genetics. In 2012, he joined the Department of Statistical Science, University College London, as a post-doctoral research associate in statistics, and in 2014 he joined the Department of Statistics, University of Warwick, as a research fellow in statistics. Since 2015 he has been a lecturer in the School of Mathematics and Statistics, University of Glasgow, Scotland.

The research interests of Dr Papamarkou include computational statistics, Bayesian methodology, Markov Chain Monte Carlo (MCMC) methods, and machine learning. Dr Papamarkou is involved in collaborations spanning domains of applications such as statistical genetics, cell and systems biology, chaos communications and signal processing.

Atsushi Uchida (S'97–M'00) received the B.S., M.S. and Ph.D. degrees in Electrical Engineering from Keio University, Yokohama, Japan, in 1995, 1997, and 2000, respectively.

In 2000, he joined the Department of Electronics and Computer Systems, Takushoku University, Tokyo, Japan, where he was a Research Associate. He was a Visiting Researcher at the ATR Adaptive Communications Research Laboratories, Kyoto, Japan, from 2001 to 2002. He was a JSPS Postdoctoral Fellow at the University of Maryland, College Park, USA, from 2002 to 2004. He was a Lecturer at the Department of Electronics and Computer Systems, Takushoku University, Tokyo, Japan, from 2005 to 2008. He was an Associate Professor at the Department of Information and Computer Sciences, Saitama University, Saitama, Japan, from 2008 to 2015. Since 2015, he has been a Professor at the Department of Information and Computer Sciences, Saitama University, Saitama, Japan. He is currently working on synchronization of chaotic lasers and its applications for optical secure communications, secure key generation using chaotic lasers for cryptography, fast physical random number generation using chaotic lasers, and synchronization of chaos and consistency in nonlinear dynamical systems.

Dr. Uchida is a member of the Optical Society of America, American Physical Society, the Institute of Electronics, Information, and Communication Engineers of Japan, the Japan Society of Applied Physics, the Laser Society of Japan, and the Optical Society of Japan.